



# Simultaneous investigation of hydrodynamic characteristics and column mass recovery of waste water of spearmint produced in a hydro-distillation using RDC extraction column

Elnaz Jafari Ozumchelouei, Hossein Bahmanyar, and Sepideh Mansoori

5 Surface Phenomena and Liquid-Liquid Extraction Research Lab, School of chemical Engineering, University College of engineering, University of Tehran, Tehran, Iran

## ABSTRACT

10 A rotary disk contactor (RDC) has been used to investigate the mass recovery of essential oil (EO) in the waste water from hydro-distillation of the spearmint plant by using *n*-hexane. Amount of mass recovery indicates a proper performance of the RDC. Results show that an increase in rotor speed, dispersed phase flow rate, and nozzle size lead to the mass recovery enhancement. A new correlation has been developed adopting response surface methodology through a Box–Behnken design for the prediction of the mass recovery as a function of rotor speed, dispersed phase flow rate, and nozzle size.

## ARTICLE HISTORY

Received 20 April 2018  
Accepted 14 November 2018

## KEYWORDS

RDC column; mass recovery; Box–Behnken design (BBD); extraction; essential oil

## 15 Introduction

Herbs are one of the most substantial resources of medicine that human beings have used for many years, and their significance is increasing day by day.<sup>[1]</sup> Currently, extensive research is done about medicinal plants and natural-drug-based medicines. The presence of secondary compounds in these plants imparts some intriguing medicinal properties to them.

20 Secondary metabolites encompass a range of commercial compounds such as alkaloids, sapiens, steroids, essential oils (EOs), and so on, among which, drug compounds and EOs are of particular importance. In fact, these compounds are produced in plants for two main purposes: (1) to improve their compatibility with environmental conditions and (2) to protect the plants against pathogenic agents, pests, etc.<sup>[2]</sup>

30 *Lamiaceae* family is one of the greatest herbal families that has spread over most areas of the Earth, comprising 200 genera and more than 3000 species.<sup>[3]</sup> The *Mentha* genus, which includes 25–30 species, can be found in the moderate regions of Asia, Europe, Australia, and South Africa.<sup>[4]</sup> *Mentha spicata* L., known as spearmint with abbreviated name mint, is one of the most functional medicinal plants in the *Mentha* family on account of its EO and valuable therapeutic characteristics.<sup>[3]</sup> The spearmint is a perennial herbaceous, glabrous plant with rectangular jagged leaves.<sup>[5]</sup>

EOs like spearmint EO are mixtures of organic compounds that are dominated by the terpenes, the terpenoids, and oxygen containing derivatives of the terpenes; they can be dissolved in alcohol and other organic solvents.<sup>[6,7]</sup>

Spearmint EO is rich in carvone which gives off odor spearmint. The highest amount of carvone can be found in the EO extracted from young leaves.<sup>[8]</sup> The carvone is a monoterpene ketone which has two enantiomers: (*S*)-(+)-carvone (existing in caraway EO) and (*R*)-(–)-carvone (major component in spearmint EO). (*R*)-(–)-Carvone has some usage in pharmacological fields, e.g., antinociception, and reducing peripheral nervous activity.<sup>[9]</sup> Other major components are limonene, 1,8-cineole, caryophyllene.<sup>[10]</sup> Spearmint EOs are widely applied in food, cosmetics, beverage, and pharmaceutical industries.<sup>[11]</sup>

The extraction process of EOs is not the same for all plants; since the EOs feature different compositions, each of them must be extracted by employing its own proper approach. As far as industrial production is concerned, there are three general methods for extracting EOs: hydro-distillation, organic solvent extraction, and maceration techniques.<sup>[12,13]</sup>

Hydro-distillation is a much gentler technique of achieving EOs from dried leaves.<sup>[14]</sup> In this method, a large amount of waste water remains, which according to the gas chromatography–mass spectrometry

(GC–MS) analysis contains considerable proportions of active ingredients. Therefore, coming up with a suitable approach for the recycling of the residue EO and active ingredients in the waste water from hydro-distillation seems quite imperative when it comes to industrial applications and environmental issues.

Liquid–liquid extraction has been taken for decades to separate soluble components in liquid mixtures by contacting the incompatible solvents;<sup>[15]</sup> it also is considered as the most used operating unit in petrochemical, pharmaceutical, and chemical industries.<sup>[16,17]</sup> One of the major extraction columns is rotary disk contactor (RDC) which has been widely utilized in chemical and petroleum industries thanks to its benefits such as high efficiency per unit height, low energy consumption, low driving force, simple construction, and ease of operation.<sup>[18–20]</sup>

In the present study, for the first time, the liquid–liquid extraction method (using RDC), for the separation of EO in the waste water from hydro-distillation of the spearmint plant, has been investigated in a laboratory scale.

Since the choice of solvent is a key factor in liquid–liquid extraction, *n*-hexane was selected due to its capability of dissolving the components of EOs and the active ingredients of the plants, low boiling point, the proper density difference with water, and poor solubility in water.<sup>[21,22]</sup>

Moreover, hydrodynamic parameters such as static hold-up and drop size were studied and the effects of operational and geometrical parameters, *i.e.*, rotor speed, dispersed phase flow rate, and nozzle size on the column mass recovery, were analyzed. In order to reduce the number of experiments, costs, and time, design of experiments (DOE) method was put into practice.

## Experimental

### Experimental setup

The schematic and picture of RDC column used for the present work are shown in Fig. 1. The column was actually a cylindrical glass, and its internal parts (rotor, stator, and shaft) were made of stainless steel. The main section was constructed of Pyrex glass with internal diameter and height of 143 and 6.4 cm, respectively. The column consisted of 13 stages that were agitated using an electromotor. Table 1 indicates the characteristics of the column.

### Liquid–liquid system

All experiments were accomplished in a liquid–liquid system at ambient temperature. Waste water was

applied as the continuous phase and *n*-hexane were used as the dispersed phase for all tests. The main physical properties of these systems are listed in Table 2.

For measuring viscosity and surface tension, Viscometer (SCHOTT-GREATER GmbH, Germany) and digital tensiometer K10T (KRUS GmbH, Germany) were used. By determining the mass of laboratory flask containing intended liquid with distinctive volume and at specific temperature, density was calculated.

### Operating variable

In this research, three operational parameters including rotor speed, volumetric flow rate of dispersed phase, and nozzle size were taken into account. For each experiment, the operating variables were systematically varied to determine their influence on the mass recovery, mean drop size, and hold-up. The examined operating conditions are detailed in Table 3.

### Experimental procedure

In this study, the continuous phase was the waste water from the hydro-distillation of spearmint. For this purpose, before conducting the experiments, in order to produce continuous phase, plant material (5.5 kg) was placed into the still tank and then filled up with water in 1:20 w/v (kg/L) ratio and distilled for 6 h. The schematic of the pot still used for the present work is shown in Fig. 2.

Prior to running the column, dispersed phase was saturated with distilled water. At the beginning of each run, column was filled up with waste water to a certain height and flow rate set at the specific value. Afterward, rotor speed was adjusted to the specified level with the aid of a digital motor drive. Then, *n*-hexane was injected from the bottom of the column via the glass nozzle, and flow rate was adjusted to the desired amount. Flow rates of both phases were measured through the rotameters.

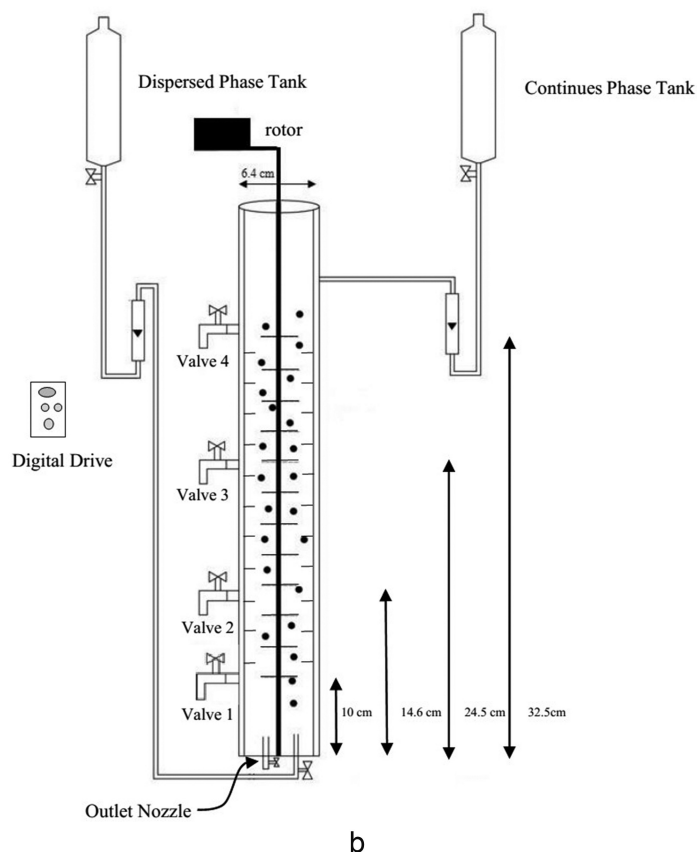
### Method

#### GC–MS analysis

The chemical analysis of the EOs and samples constituents was performed using an Agilent Technologies 7890A gas chromatograph and a 5975C VL MSD with triple-axis detector as a mass selective detector. The GC was equipped with a 30 m × 0.25-mm silica capillary Rtx 5 MS column, with a 25-μm film thickness. The oven temperature program initiated at 40°C, then rose



a



b

Figure 1. (a) Picture and (b) schematic of RDC column.

Table 1. Characteristics of the column.

Geometrical parameters	Values
Column internal diameter ( $d_T$ )	6.4 cm
Stator internal diameter ( $d_s$ )	4.35 cm
Rotor diameter ( $d_r$ )	3.24 cm
Column height	143 cm
Active height ( $H$ )	32.5 cm
Compartment height ( $h_c$ )	2.24 cm
Number of compartment	13
Rotor and stator thickness	0.8 mm
Number of valves	4

Table 2. Physical properties of the systems studied at 25°C.

Compound	Density (kg/m <sup>3</sup> )	Viscosity (N s/m <sup>2</sup> )	Surface tension (N/m)
Waste water produced from hydro-distillation of spearmint	992.3	0.001	0.072
<i>n</i> -Hexane (solvent)	659.4	0.00031	0.01719

to 250°C at the rate of 3°C/min, while the injector temperature and detector temperature were 250 and 230°C, respectively. The carrier gas was He (99.999%),

Table 3. Range of operating variables.

Range of operating variables			
$Q_d$ (cc/min)	$Q_c$ (cc/min)	$N$ (rpm)	Nozzle size (mm)
3, 7.5, 10, 20, 30, 35	78	75, 125, 175, 225	0.8, 1, 1.2

with a flow rate of 50 mL/min. Mass spectra were taken at 70 eV. The injected sample volume was 0.4  $\mu$ L in a split mode. Compounds were characterized by their GC retention time relative to the known compounds, with the help of Agilent MSD Chemstation (Rev E.02.02. 1413).

### Mass recovery calculation

In each experiment, *n*-hexane (saturated with distilled water) as the dispersed phase was injected from the bottom of the column into the waste water as the continuous phase. The flow pattern in the column was counter current. As the dispersed phase droplets

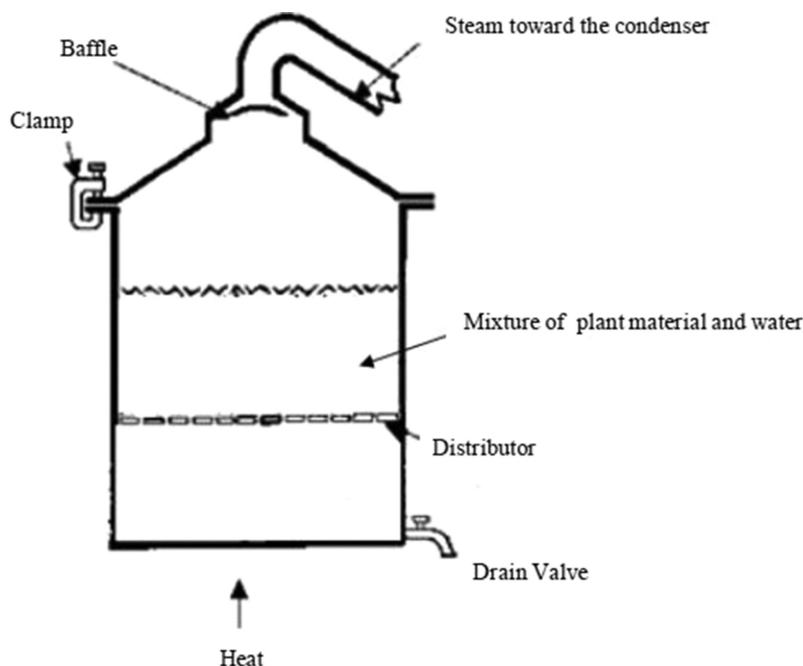


Figure 2. Schematic of pot still.

were ascending in the column, the EO was being transferred from the continuous phase into the dispersed phase. At the end of each run, sample of organic phase was taken at specific height (from valve 4) and then was concentrated at ambient temperature (by natural evaporation). The solute weight percentage was determined by GC-MS analysis. The concentration values of the EO components in each test were obtained by the following equation (Eqs. 1 and 2):

$$C_i = \frac{\omega_i}{Mw_i} * \rho_{\text{solution}} \quad (1)$$

where  $\omega$  is weight percentage of components.

The mass transfer performance is expressed as

$$E = \frac{\text{amount of mass transfer}}{\text{maximum possible mass transfer}} = \frac{C_0 - C_i}{C_0 - C_i^*} \quad (2)$$

where  $C_0$  is the initial concentration which is zero for pure *n*-hexane and  $C_i^*$  is found experimentally.

#### Measurement of drop size

In order to measure drop size, the photography approach (via a Canon 6 XIS camera) was applied. In each experiment, with the stabilized conditions, several photos of the inside of the column at different stages along the active height were taken. These photos were investigated taking advantage of ImageJ analysis software. For the estimation of drop size, the drops were

compared with the size of the stators, rotors thickness, or central shaft outside diameter, which were selected as the reference, then the diameter of drops was evaluated directly. Most of droplets were spherical; for elliptical drops, the major and minor axes ( $d_1$  and  $d_2$ ) were measured and following equation was used to calculate the equivalent diameter,  $d_e$ :

$$d_e = (d_1^2 d_2)^{(1/3)} \quad (3)$$

Finally, about 200 drops were analyzed for each test. The Sauter-mean drop diameter was calculated through Eq. 4:

$$d_{32} = \frac{\sum_{i=1}^n n_i d_i^3}{\sum_{i=1}^n n_i d_i^2} \quad (4)$$

where  $n_i$  is the number of drops of diameter  $d_i$ .

A picture of droplets is given in Fig. 3.

#### Measurement of static dispersed-phase hold-up

All of the experiments were designed far from flooding conditions. The dispersed phase hold-up was determined by the shutdown method, in which, at the end of each run, the continuous and dispersed inlet and outlet valves were closed and electromotor was turned off at the same time. After a certain period of time (about 10 min) and with the coalescence of the dispersed phase drops, in order to evaluate the local static hold-up, at first, the dispersed phase (collected at the top of the column) was drained, and then, the whole liquid volume was discharge from the bottom of the column. Later, the volume of the aqueous phase and the organic phase was specified by means of a decanter. The

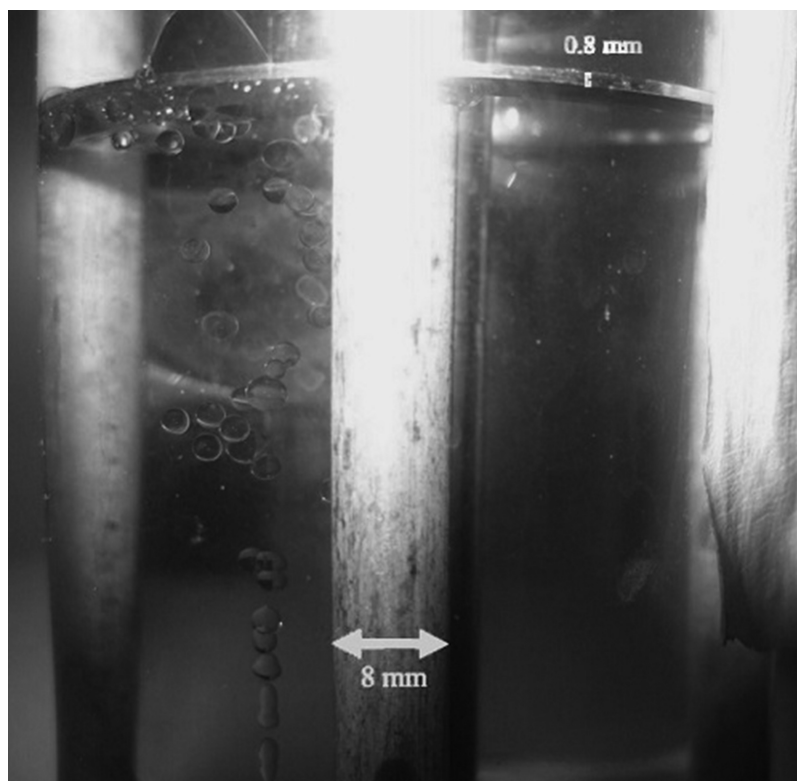


**Figure 3.** Picture of droplets after changing the contrast of background.

225 static hold-up would be calculated by the ratio of the  
 organic phase volume to the total volume of the extraction  
 zone. A picture of static hold-up is shown in Fig. 4.

#### DOEs

230 With the aim of reducing the number of experiments and  
 costs and economizing on the time, DOE using “Design-  
 Expert 7.0.0 Trial” (Stat-Ease Inc., Minneapolis) was  
 employed. Mass recovery was developed based on a three-  
 level-three-factor Box–Behnken design (BBD) consisting of  
 17 experimental tests (including 5 repetitions at the central  
 235 point). The effects of the rotor speed, the dispersed phase

flow rate, and the nozzle size on the mass recovery were  
 statistically assessed. Table 4 shows the experimental levels  
 of the factors and Table 5 presents the design matrix for the  
 Box–Behnken method.

## Result and discussion

240

### *Characterization of the volatile constituents of the spearmint plant*

Chemical composition of spearmint EO was charac-  
 terized by GC–MS analysis, through the comparison

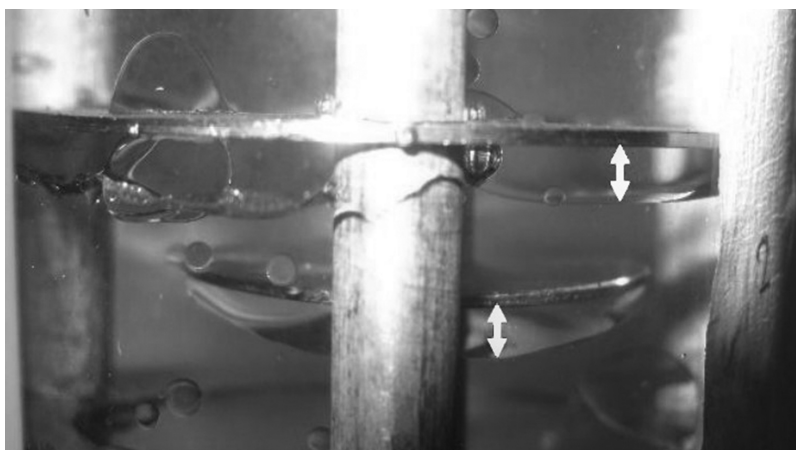


**Figure 4.** Picture of static hold up under rotor and stator after changing the contrast of background.



**Table 4.** Experimental levels of the factors used in Box–Behnken method.

Factors (parameters)	Factors levels			
		–1	0	1
Rotor speed (rpm)	A	125	175	225
Dispersed phase flow rate (cc/min)	B	10	20	30
Nozzle size (mm)	C	0.8	1	1.2

**Table 5.** Design matrix for Box–Behnken method.

Run number	A: <i>N</i> (rpm)	B: <i>Q<sub>d</sub></i> (cc/min)	C: Nozzle size (mm)
1	225	30	1
2	175	20	1
3	225	20	0.8
4	175	10	1.2
5	225	20	1.2
6	125	10	1
7	175	20	1
8	175	20	1
9	125	20	0.8
10	225	10	1
11	125	30	1
12	175	30	0.8
13	125	20	1.2
14	175	30	1.2
15	175	20	1
16	175	10	0.8
17	175	20	1

**Table 6.** Component of spearmint essential oil.

Number	Compound	RT (min)	%w
1	Alpha-pinene	9.021	0.685
2	Sabinene	10.712	0.64
3	Beta-pinene	10.814	1.148
4	Beta-myrcene	11.536	0.386
5	3-Octanol	11.859	0.197
6	Alpha-terpinene	12.615	1.242
7	<i>p</i> -Cimene	13.005	0.229
8	Limonene	13.252	8.871
9	1,8-Cineole	13.371	4.252
10	Gama-terpinene	14.594	2.344
11	<i>cis</i> -Sabinenehydrate	15.036	0.657
12	Alpha-terpineolene	15.936	0.304
13	<i>p</i> -Ment-2- <i>n</i> -1-ol	17.542	0.434
14	Menthone	19.020	0.234
15	Delta-terpineol	19.734	0.256
16	Terpinen-4-ol	20.184	2.723
17	Alpha-terpineol	20.915	0.928
18	Dihydrocarvone	21.195	7.726
19	<i>trans</i> -Carveol	22.427	0.312
20	Carvone	23.633	35.148
21	Beta-bourbonene	29.291	3.719
22	<i>trans</i> -caryophyllene	30.761	7.38
23	Alpha-humulene	32.103	0.86
24	Germacrene- $\delta$	32.621	2.85
25	Bicyclogermacrene	33.878	1.416
26	Spatulenol	37.175	2.792
27	Caryophyllene oxide	37.345	4.95
28	Alpha-cadinol	39.468	1.945
	Total identified		94.328

RT: Retention time.

of the mass spectra of oil constituents with the mass spectra from the Wiley 7N data library. As shown in Table 6, 28 compounds including more than 94% of the total hydro-distillation EO were characterized. The major constituents were carvone (35.148%), limonene (8.871%), dihydrocarvone (7.726%), and *trans*-caryophyllene (7.38%).

### Mass recovery

At the end of each test, the composition of the prepared sample was detected by GC–MS analysis, and then the concentration of EO in the sample was calculated by Eq. 1. The concentration of carvone, as a major compound, is given in Table 7. Consequently, the mass recovery of the RDC column was obtained by Eq. 2. The results were summarized in Table 7. As can be seen in this table, the amount of mass recovery is varied between 34.26% and 59.07%. Runs number 1 and 6 have the highest and the lowest values of mass recovery, respectively. The final value of concentration or the saturated value of concentration in organic phase is found experimentally ( $C^* = 0.066$  mol/L).

### Investigation of hydrodynamic parameters

#### Drop size

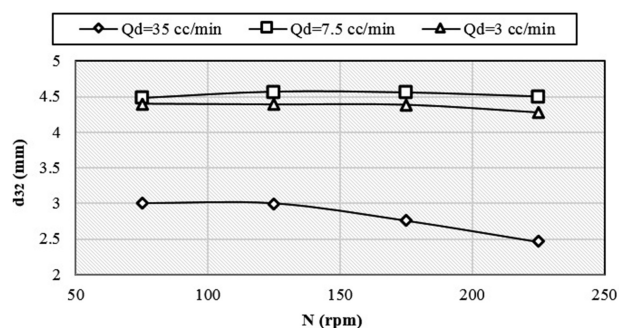
In the current study, the drop size was investigated under various operating conditions including rotor speed, dispersed phase flow rate, and nozzle size.

**Table 7.** The concentration of carvone and mass recovery of RDC column.

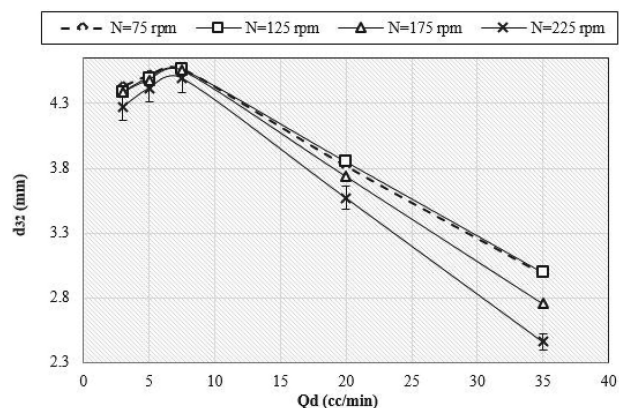
Run number	A: <i>N</i> (rpm)	B: <i>Q<sub>d</sub></i> (cc/min)	C: Nozzle size (mm)	<i>C<sub>carvone</sub></i> (mol/L)	% <i>E</i> (response)
1	225	30	1	0.03899	59.07
2	175	20	1	0.03344	50.67
3	225	20	0.8	0.03580	54.24
4	175	10	1.2	0.03187	48.29
5	225	20	1.2	0.03658	55.42
6	125	10	1	0.02261	34.26
7	175	20	1	0.03256	49.33
8	175	20	1	0.03286	49.78
9	125	20	0.8	0.02426	36.75
10	225	10	1	0.03173	48.07
11	125	30	1	0.03035	45.98
12	175	30	0.8	0.03380	51.21
13	125	20	1.2	0.03034	45.96
14	175	30	1.2	0.03648	55.27
15	175	20	1	0.03203	48.53
16	175	10	0.8	0.02710	41.06
17	175	20	1	0.03483	52.77

Figure 5 shows the effect of rotor speed on Sauter mean drop size. It can be seen that the drop size decreases by increasing rotor speed. In fact, by increasing rotor speed, due to a rise in turbulence and shear stress forces on drops and reduction in the critical drop diameter, drop break-up will multiply. So, drop diameter and consequently the Sauter mean drop size will decline.

According to Fig. 6, by increasing the dispersed phase flow rate, first, the Sauter mean drop size, due to creation bigger mother droplet, exhibits an upward trend until it reaches its maximum size, after which by increasing the dispersed phase flow rate (owing to a shift in the flow rate from single drop to jet and a reduction in the drop



**Figure 5.** Variation of  $d_{32}$  versus rotor speed at different dispersed phase flow rates and nozzle size 0.8 mm.



**Figure 6.** Variation of  $d_{32}$  versus dispersed phase flow rate at different rotor speeds and nozzle size 0.8 mm.

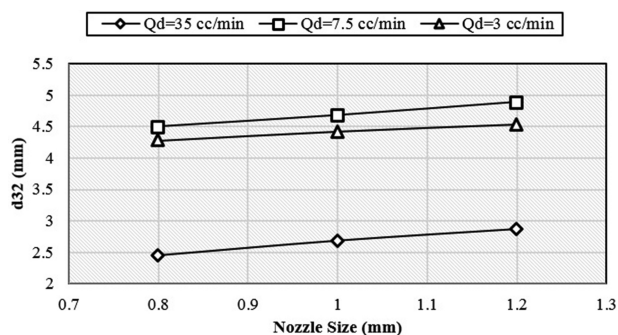
formation time), the drop diameter and consequently the Sauter mean drop size will decrease. The experiments have been repeated just to be confident about the accuracy of the results. Regarding the error rate that might exist in the experiments, error bar is shown in one of the experimental results in Fig. 6.

As shown in Fig. 7, by increasing the nozzle size, because of the formation of bigger mother drop, the Sauter mean drop size will grow.

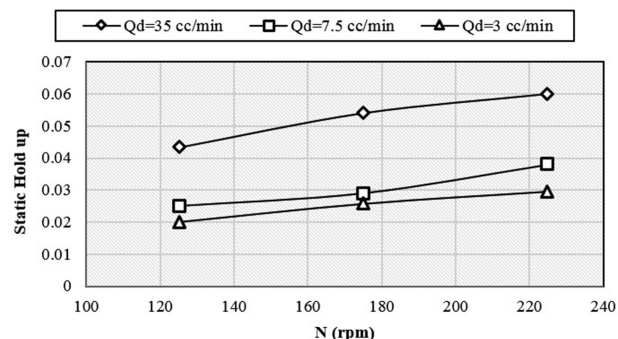
### Static hold-up

In these experiments, the effect of rotor speed, dispersed phase flow rate, and nozzle size on static hold-up were studied.

Regarding to Fig. 8, the dispersed phase static hold-up significantly increases as the rotor speed picks up. The increase in the rotor speed raises the number of drops in the column due to higher occurrence of drop break-up. In addition, by elevating the rotor speed, the frequency of drop collisions with the internal parts of the RDC column increased. Accordingly, as the number of drops with high frequencies of drop collisions grew, the probability of the entrapment of droplets under the rotors and stators in the RDC column increased.



**Figure 7.** Variation of  $d_{32}$  versus nozzle size at different dispersed phase flow rates and  $N = 225$  rpm.



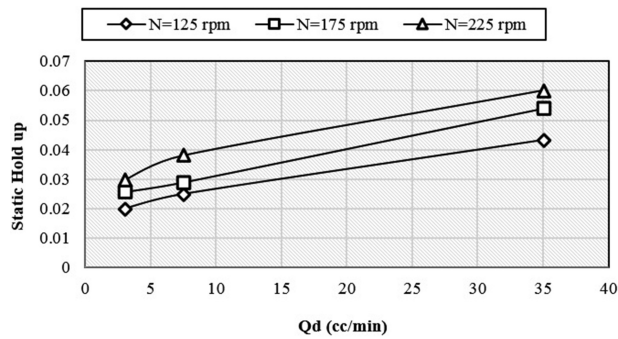
**Figure 8.** Variation of static hold up versus rotor speed at different dispersed phase flow rates and nozzle size 0.8 mm.

Figure 9 illustrates the effect of the dispersed phase flow rate on static hold-up. This figure shows an increase in the static hold-up with increasing the dispersed phase flow rate; this happened because of the rise in the dispersed phase content in the column.

The effect of the nozzle size on static hold-up is shown in Fig. 10. An increase in nozzle size results in an increase in static hold-up, owing to the formation of bigger mother drops, which leads to a decline in the first and second critical rotor speed and an increase in drop breakage; this, in turn, multiplies the number of drops, causing the probability of droplet entrapment between the internal part of the column to rise.

### Development of a model using BBD

BBD was used for the investigation of the effect of parameters on the mass recovery of RDC column and development of a model. In order to decide on a proper response surface model, analysis of variance table was taken into account, as shown in Table 8. The model  $F$ -value of 64.27 indicates that the model is significant. There is only a 0.01% chance that such a large “model  $F$ -value” could occur due to noise. Values of “prob >  $F$ ”



**Figure 9.** Variation of static hold up versus dispersed phase flow rate at different rotor speeds and nozzle size = 0.8 mm.

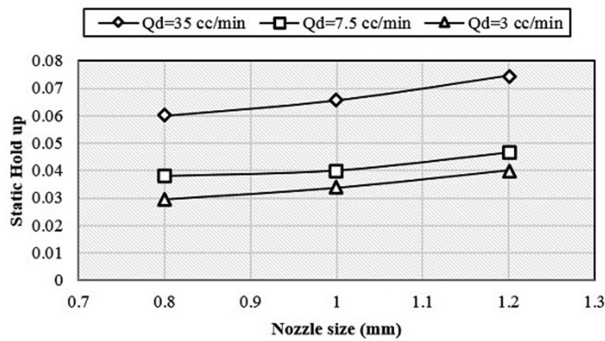


**Figure 10.** Variation of static hold up versus nozzle size at different dispersed phase flow rates and  $N = 225$  rpm.

for the model terms are  $<0.0001$ , suggesting that the model terms are statistically meaningful. From Table 8 it can be deduced that A, B, C, AC,  $A^2$  are significant model terms. The “lack of fit  $F$ -value” of 0.42 implies that the lack of fit (LOF) is not significant relative to the pure error. There is a 83.58% chance that a “lack of fit  $F$ -value” this large could take place owing to noise. Thus, the model equation is quite adequate for the predication of the mass recovery. A quadratic response surface model was chosen to fit the empirical data, in view of its higher  $F$ -value and  $R$ -value and lower LOF and prediction error sum of squares.

Other statistical parameters of the quadratic model are given in Table 9. The “pred  $R$ -squared” of 0.9471 is

**Table 9.** Statistical parameters for the quadratic model.

Std. dev.	0.01311124	$R$ -squared	0.974721346
Mean	0.486301248	Adj. $R$ -squared	0.959554154
CV %	2.696114723	Pred $R$ -squared	0.947095967
PRESS	0.003597678	Adeq precision	27.84629796

in reasonable agreement with the “adj.  $R$ -squared” of 0.9596. “adeq precision” measures the signal-to-noise ratio. The ratio of 27.846 points to an adequate signal. The value of standard deviation is 0.013, emphasizing the model is acceptable, too. This model can be made use of to navigate the design space.

Final equation in terms of coded factors is shown in Eq. 5:

$$E = 0.50 + 0.067 \times A + 0.050 \times B + 0.027 \times C - 0.020 \times A \times C - 0.021 \times A^2 - 0.013 \times B^2 \quad (5)$$

Final equation in terms of actual factors is shown in Eq. 6:

$$E = -0.62922 + 6.31483 \times 10^{-3} \times N + 0.010004 \times Q_d + 0.48684 \times \text{Nozzlesize} - 2.00758 \times 10^{-3} \times N \times \text{Nozzlesize} - 8.46013 \times 10^{-6} \times N^2 - 1.255 \times 10^{-4} \times Q_d^2 \quad (6)$$

### Effects of rotor speed, dispersed phase flow rate, and nozzle size on the mass recovery

The response surface plots were obtained between two independent variables and the response variable, while keeping the third variable fixed at a central level. The following figures illustrate the positive effects of these parameters on the mass recovery. Figure 11a displays the effect of rotor speed and dispersed phase flow rate on mass recovery. As expected, an increase in the rotor speed leads to a decrease in the Sauter mean drop diameter; so interfacial area gets enhanced. However, the reduction in drop diameter brings about a deterioration in the overall mass transfer coefficient, on account of the diminished internal circulations

**Table 8.** Analysis of variance (ANOVA) table of the quadratic response surface model.

Source	Sum of squares	df	Mean square	$F$ -value	$p$ -Value prob > $F$	
Model	0.066	6	0.011	64.27	<0.0001	Significant
A— $N$	0.036	1	0.036	210.85	<0.0001	
B— $Q_d$	0.02	1	0.02	115.55	<0.0001	
C—Nozzle size	0.005876	1	0.005876	34.18	0.0002	
AC	0.001612	1	0.001612	9.38	0.012	
$A^2$	0.001889	1	0.001889	10.99	0.0078	
$B^2$	0.0006652	1	0.0006652	3.87	0.0775	
Residual	0.001719	10	0.0001719			
Lack of fit	0.0006647	6	0.0001108	0.42	0.8358	Not significant
Pure error	0.001054	4	0.0002636			
Cor total	0.068	16				



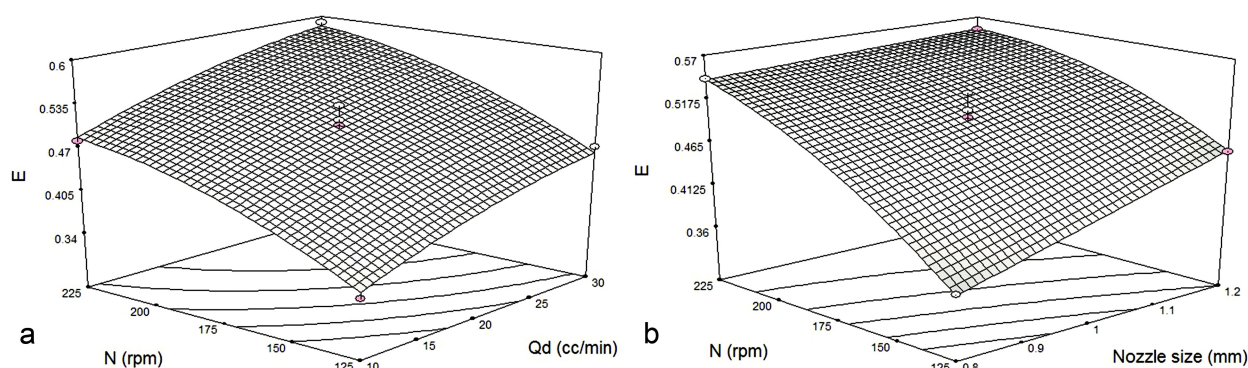


**Figure 11.** Response surface plots: (a) effect of rotor speed and dispersed phase flow rate at constant nozzle size (1 mm) and (b) effect of rotor speed and nozzle size at constant dispersed phase flow rate (20 cc/min) on mass recovery.

inside the drop. It can be inferred from the results that the effect of interfacial area is more influential than the overall mass transfer coefficient, and hence the mass recovery goes up as the rotor speed increases. With respect to Fig. 11a, by accelerating the dispersed phase flow rate, due to a reduction in the drop diameter, and the subsequent enhancement of the interfacial area, the mass recovery experiences improvement.

Figure 11b shows the effect of rotor speed and nozzle size on mass recovery. With regard to Fig. 11a,b, the rotor speed and the nozzle size have the highest and lowest impacts on mass recovery, respectively.

## Conclusion

In the current study, waste water was produced from hydro-distillation of spearmint plant, and with reference to the GC-MS analysis, it includes noticeable amount of EO and active ingredient. The carvone concentration, as a dominant component, was 0.066 mol/L. The mass recovery performance of the EO from the waste water was examined in a RDC column using *n*-hexane as the solvent. The effect of different parameters on the mass recovery performance, static hold-up, and Sauter mean drop diameter was assessed. The experimental observation confirmed that the column mass recovery was boosted by increasing the rotor speed, the dispersed phase flow rate, and the nozzle size, among which the rotor speed has the highest impact. The maximum mass recovery in all of the tests was 59.07%, which demonstrates the successful application of the liquid-liquid extraction process and the satisfactory performance of the RDC column in recovery of the essence from the waste water using *n*-hexane. An equation for prediction of mass recovery was presented in terms of rotor speed, dispersed phase flow rate, and nozzle size by adopting BBD. In addition, our findings suggested that Sauter mean drop diameter

lessened by increasing the rotor speed and the dispersed phase flow rate and increased by selecting larger nozzles.

## Nomenclature

$N$	Rotor speed (rpm)	
$d_r$	Rotor diameter (m)	410
$d_s$	Inner stator diameter (m)	
$D$	Column diameter (m)	
$H$	Column height (m)	
$h_c$	Compartment height (m)	
$d_i$	Drop size (mm)	415
$V_c$	Superficial velocity of continuous phase (m/s)	
$V_d$	Superficial velocity of dispersed phase (m/s)	
$Q$	Volumetric flow rate	
$\omega$	Mass fraction	
$M_w$	Molecular weight	420

## Subscript

C	Continuous phase	
D	Dispersed phase	
I	Component number	
*	Final concentration or saturated value of concentration	425

## Greek letters

$\Phi$	Hold-up	
$P$	Density ( $\text{kg/m}^3$ )	
$\Sigma$	Interfacial tension between two phases (N/m)	

## References

- [1] Tonthubthimthong, P.; Chuaprasert, S.; Douglas, P.; Luewisutthichat, W. (2001) Supercritical  $\text{CO}_2$  extraction of nimbin from neem seeds—an experimental study. *Journal of Food Engineering*, 47 (4): 289–293. doi: 10.1016/S0260-8774(00)00131-X.
- [2] Bakkali, F.; Averbeck, S.; Averbeck, D.; Idaomar, M. (2008) Biological effects of essential oils— a review.

*Food and Chemical Toxicology*, 46 (2): 446–475. doi: [10.1016/j.fct.2007.09.106](https://doi.org/10.1016/j.fct.2007.09.106).

- 440 [3] Ansari, K.; Goodarznia, I. (2012) Optimization of  
supercritical carbon dioxide extraction of essential oil  
from spearmint (*Mentha spicata* L.) leaves by using  
Taguchi methodology. *The Journal of Supercritical  
Fluids*, 67: 123–130. doi: [10.1016/j.supflu.2012.03.011](https://doi.org/10.1016/j.supflu.2012.03.011).
- 445 [4] de Sousa Barros, A.; de Morais, S.M.; Ferreira, P.A.T.;  
Vieira, Í.G.P.; Craveiro, A.A.; Dos Santos Fontenelle, R.  
O.; ... de Sousa, H.A. (2015) Chemical composition  
and functional properties of essential oils from mentha  
species. *Industrial Crops and Products*, 76: 557–564.  
doi: [10.1016/j.indcrop.2015.07.004](https://doi.org/10.1016/j.indcrop.2015.07.004).
- 450 [5] Chrysargyris, A.; Xylia, P.; Botsaris, G.; Tzortzakakis, N.  
(2017) Antioxidant and antibacterial activities, mineral  
and essential oil composition of spearmint (*Mentha  
spicata* L.) affected by the potassium levels. *Industrial  
Crops and Products*, 103: 202–212. doi: [10.1016/j.  
indcrop.2017.04.010](https://doi.org/10.1016/j.indcrop.2017.04.010).
- 455 [6] Araus, K.; Uquiche, E.; Del Valle, J.M. (2009) Matrix  
effects in supercritical CO<sub>2</sub> extraction of essential oils  
from plant material. *Journal of Food Engineering*, 92  
460 (4): 438–447. doi: [10.1016/j.jfoodeng.2008.12.016](https://doi.org/10.1016/j.jfoodeng.2008.12.016).
- [7] Reverchon, E.; (1997) Supercritical fluid extraction  
and fractionation of essential oils and related  
products. *The Journal of Supercritical Fluids*, 10 (1):  
1–37. doi: [10.1016/S0896-8446\(97\)00014-4](https://doi.org/10.1016/S0896-8446(97)00014-4).
- 465 [8] Chauhan, R.; Kaul, M.; Shahi, A.; Kumar, A.; Ram, G.;  
Tawa, A. (2009) Chemical composition of essential oils in  
mentha spicata L. accession [IIIM (I) 26] from  
North-West Himalayan region, India. *Industrial Crops  
and Products*, 29 (2): 654–656. doi: [10.1016/j.  
indcrop.2008.12.003](https://doi.org/10.1016/j.indcrop.2008.12.003).
- 470 [9] Nogoceke, F.P.; Barcaro, I.M.; de Sousa, D.P.;  
Andreatini, R. (2016) Antimanic-like effects of (R)-(-)-  
carvone and (S)-(+)-carvone in mice. *Neuroscience  
Letters*, 619: 43–48. doi: [10.1016/j.neulet.2016.03.013](https://doi.org/10.1016/j.neulet.2016.03.013).
- 475 [10] Telci, I.; Demirtas, I.; Bayram, E.; Arabaci, O.;  
Kacar, O. (2010) Environmental variation on aroma  
components of pulegone/piperitone rich spearmint  
(*Mentha spicata* L.). *Industrial Crops and Products*, 32  
(3): 588–592. doi: [10.1016/j.indcrop.2010.07.009](https://doi.org/10.1016/j.indcrop.2010.07.009).
- 480 [11] Dai, J.; Orsat, V.; Raghavan, G.S.V.; Yaylayan, V.  
(2010) Investigation of various factors for the extrac-  
tion of peppermint (*Mentha piperita* L.) leaves. *Journal  
of Food Engineering*, 96: 540–543. doi: [10.1016/j.  
jfoodeng.2009.08.037](https://doi.org/10.1016/j.jfoodeng.2009.08.037).
- 485 [12] Reverchon, E.; De Marco, I. (2006) Supercritical fluid  
extraction and fractionation of natural matter. *The  
Journal of Supercritical Fluids*, 38 (2): 146–166. doi:  
[10.1016/j.supflu.2006.03.020](https://doi.org/10.1016/j.supflu.2006.03.020).
- [13] Weinhold, T.D.S.; Bresciani, L.F.; Tridapalli, C.W.;  
Yunes, R.A.; Hense, H.; Ferreira, S.R. (2008) Polygala  
490 cyparissias oleoresin: comparing CO<sub>2</sub> and classical  
organic solvent extractions. *Chemical Engineering and  
Processing: Process Intensification*, 47 (1): 109–117. doi:  
[10.1016/j.cep.2007.08.007](https://doi.org/10.1016/j.cep.2007.08.007).
- [14] Lucchesi, M.E.; Chemat, F.; Smadja, J. (2004) Solvent-  
495 free microwave extraction of essential oil from aromatic  
herbs: comparison with conventional hydro-distillation.  
*Journal of Chromatography A*, 1043 (2): 323–327.
- [15] Hemmati, A.; Shirvani, M.; Torab-Mostaedi, M.;  
Ghaemi, A. (2016) Mass transfer coefficients in a  
500 perforated rotating disc contactor (PRDC). *Chemical  
Engineering and Processing: Process Intensification*, 100:  
19–25. doi: [10.1016/j.cep.2015.11.011](https://doi.org/10.1016/j.cep.2015.11.011).
- [16] Rouina, S.; Abdeh, H.; Bahmanyar, H.; Sadr, A. (2016)  
Investigating the effect of nanoparticles on the dispersed  
505 phase mass transfer coefficient in a rotary disc column.  
*Chemical Engineering and Processing: Process  
Intensification*, 104: 84–93. doi: [10.1016/j.cep.2016.03.002](https://doi.org/10.1016/j.cep.2016.03.002).
- [17] Torab-Mostaedi, M.; Asadollahzadeh, M.; Safdari, J.  
(2017) Prediction of mass transfer coefficients in an  
510 asymmetric rotating disk contactor using effective  
diffusivity. *Chinese Journal of Chemical Engineering*,  
25 (3): 288–293. doi: [10.1016/j.cjche.2016.08.021](https://doi.org/10.1016/j.cjche.2016.08.021).
- [18] Hemmati, A.; Torab-Mostaedi, M.; Shirvani, M.;  
Ghaemi, A. (2015) A study of drop size distribution  
515 and mean drop size in a perforated rotating disc con-  
tactor (PRDC). *Chemical Engineering Research and  
Design*, 96: 54–62. doi: [10.1016/j.cherd.2015.02.005](https://doi.org/10.1016/j.cherd.2015.02.005).
- [19] Torab-Mostaedi, M.; Asadollahzadeh, M. (2015) Mass  
transfer performance in an asymmetric rotating disc  
520 contactor. *Chemical Engineering Research and Design*,  
94: 90–97. doi: [10.1016/j.cherd.2014.12.007](https://doi.org/10.1016/j.cherd.2014.12.007).
- [20] Shehata, A.; Elshazly, A.; Zaatout, A.; Sedahmed, G.  
(2011) Mass transfer behaviour of a new liquid-liquid  
525 rotating screen disc extractor. *Bulgarian Chemical  
Communications*, 43: 427–438.
- [21] Hidayah, N.N.; Abidin, S.Z. (2017) The evolution of  
mineral processing in extraction of rare earth elements  
530 using solid-liquid extraction over liquid-liquid extrac-  
tion: A review. *Minerals Engineering*, 112: 103–113.  
doi: [10.1016/j.mineng.2017.07.014](https://doi.org/10.1016/j.mineng.2017.07.014).
- [22] Cheng, M.-H.; Rosentrater, K.A. (2017) Economic fea-  
sibility analysis of soybean oil production by hexane  
535 extraction. *Industrial Crops and Products*, 108:  
775–785. doi: [10.1016/j.indcrop.2017.07.036](https://doi.org/10.1016/j.indcrop.2017.07.036).